Ultrasonics 91 (2019) 134–149

Contents lists available at ScienceDirect

Ultrasonics

journal homepage: www.elsevier.com/locate/ultras

# High-intensity focused ultrasound (HIFU) ablation by the frequency chirps: Enhanced thermal field and cavitation at the focus

Mingjun Wang, Yisheng Lei, Yufeng Zhou*

*School of Mechanical and Aerospace Engineering, Nanyang Technological University, Singapore*

ARTICLE INFO

*Keywords:*
High-intensity focused ultrasound (HIFU)
Frequency chirp excitation
Bubble cavitation
Temperature elevation
Lesion production

ABSTRACT

High-intensity focused ultrasound (HIFU) has become popular in the noninvasive ablation of a variety of solid tumors and cancers with promising clinical outcomes. Its ablation efficiency should be improved for the reduced treatment duration, especially for a large target. The frequency chirps were proposed and investigated for the enhanced lesion production and bubble cavitation at the focus during HIFU ablation. First, a nonlinear wave model was used to simulate the acoustic field using different excitation strategies (at the constant frequency excitation, downward and upward frequency chirps) and subsequently, the bubble dynamics and cavitation-enhanced temperature elevation were calculated by the Gilmore and Bioheat equations, respectively. Then the temperature rises and the produced lesion in the gel phantom were measured by the thermocouple and recorded photographically, respectively. Bubble activities at the focus were measured by passive cavitation detection (PCD) to quantify the scattering and inertial cavitation levels using short-time Fourier-transform (STFT). Finally, the enhanced temperature elevation, lesion production, and bubble cavitation were further confirmed in the *ex vivo* tissue samples. It is found that the frequency sweeping time plays a more important role in the enhancement of HIFU-produced lesion in the gel phantom while the frequency sweeping range seems more critical in the tissue. Altogether, large frequency sweeping range in a short time is preferable, and the frequency sweeping direction has little influence on the lesion enhancement.

## 1. Introduction

High intensity focused ultrasound (HIFU) has been emerging as a novel, noninvasive, and effective therapeutic modality on the soft-tissue sarcomas since its clinical trials in the middle 1990s [1–3]. A variety of targets have been treated with very promising results, such as the pancreas, liver, prostate, breast, and bone cancers and uterine fibroids. Initial clinical success encourages the further development of HIFU technology and its commercialization. Several HIFU systems have obtained regulatory clearance in North America (e.g., USA, Canada, Mexico, Costa Rica, and the Caribbean), Europe (e.g., UK, France, Bulgaria, Italy, Poland, Romania, Spain, and Russia), Eastern Asia (e.g., China, Korea, and Japan), Australia, and South Africa. Its major mechanism is the fast temperature elevation in the tissue over 60–65 °C due to the absorption of sufficiently high acoustic energy focused into a tight region for irreversible protein denaturation. The coagulation time of HIFU could be on the order of ten seconds to produce single-shot lesions 2 mm in diameter and 10 mm in length *in vivo* [4]. The narrow boundary between HIFU-induced necrosis and the surrounding tissue, ~200 μm [5,6], and much less acoustic intensity and lower temperature elevation out of the focal region make HIFU ablation well-controlled with little damage to the intervening tissues. In comparison to the conventional cancer treatment modalities (e.g., open surgery and radio- or chemo-therapy), HIFU has significant advantages of non-invasiveness, few complications, less in-hospital time, theoretically unlimited tissue tolerance for retreatment, improved quality of life for the advanced cancer patients with metastasis, and feasible treatment for the cancers at the anatomically difficult and complicated locations. Therefore, its acceptance by both physician and patient becomes more popular.

Besides the thermal effect, the formation and oscillation of bubbles induced by the incident ultrasound wave also have a significant effect on tissue heating in the hyperthermia applications and HIFU ablation [7]. With the presence of bubbles, a great enhancement of converting the acoustic energy to the thermal energy could be accomplished. Several studies illustrated that ultrasonically induced cavitation bubbles locally enhance tissue heating in HIFU treatment [8,9]. The stable cavitation causes the high shear stress between the bubble and the surrounding medium, and the inertial cavitation (IC) produces the shock wave, high-speed jet, and broadband noise emission. A

* Corresponding author at: School of Mechanical and Aerospace Engineering, Nanyang Technological University, 50 Nanyang Ave., Singapore 639798, Singapore.
*E-mail address:* yfzhou@ntu.edu.sg (Y. Zhou).

https://doi.org/10.1016/j.ultras.2018.08.017
Received 9 February 2018; Received in revised form 14 August 2018; Accepted 20 August 2018
Available online 21 August 2018

comparison of cavitation activities served to HIFU ablation has suggested that the enhanced heating effect was mainly from the IC for the emission of broadband noise which can be more readily absorbed [10]. A strong correlation was found between enhanced heating and the broadband emissions arising from IC.

Although acoustic cavitation plays a vital role in the ablation, the realization of bubble-assisted HIFU is not always possible due to the lack of pre-existing bubble nucleation in the tissue. High peak negative pressure (7–10 MPa) required to initiate acoustic cavitation *in vivo* makes it difficult to localize, sustain, and confine cavitation activities. Several approaches have been employed to generate the sufficient bubble cavitation. Both ultrasound contrast agents (microbubbles) and micro/nanoparticles (e.g., polystyrene spheres, liposomes, polymers, micelles, dendrimers, emulsions, and quantum dots) can provide the cavitation nuclei, decrease the cavitation threshold, and repeatedly initiate cavitation at the same location [11–14]. IC intensities of the suspension with superhydrophobic polytetrafluoroethylene nanoparticles were 10.3 and 48.4 times stronger than those of deionized water at the peak negative pressure of 2 and 5 MPa, respectively [15]. Up to 12 fold larger necrosis could be achieved with the addition of microbubbles [11]. A high intensity and short triggering HIFU pulse above the cavitation threshold was used to generate cavitation bubbles at the focus and then followed by the conventional HIFU ablation (long pulse duration but at the low acoustic intensity) to sustain the cavitation activities and enhance the heating locally and efficiently [16].

Another strategy of enhancing the bubble cavitation is to apply two or more frequencies during HIFU ablation. A high-frequency (5 MHz) excitation was applied to a tissue-mimicking phantom to induce a rapid temperature rise followed by a low-frequency (1 MHz) one to the same region to induce the acoustic cavitation [17]. Cavitation enhancement may be due to the temporary super-saturation of air in the initially air-saturated samples and the reduction of surface tension at an elevated temperature by the high-frequency HIFU. High-speed photographic observations and acoustic emission measurement by the dual-frequency ultrasound (21 kHz and 355 kHz) were made in water and dilute aqueous solutes [18]. Such nucleating effect was homogenous at the low acoustic power and highly localized at the high acoustic power. Both the fundamental high-frequency acoustic emission peaks and the high order low-frequency harmonics were significantly intensified in the dual-frequency mode with the presence of these solutes. In addition, the use of frequency chirps to probe the acoustic cavitation activities was also explored. Enhancement and quenching of HIFU-induced cavitation activity were achieved with short frequency sweeping range in positive and negative direction, respectively [19]. The frequency sweeping direction and rate govern the growth and coalescence of bubbles in the acoustic field. Furthermore, chirp coded excitation could also reduce the standing wave formation and improve focusing of transcranial ultrasound in the localized blood-brain barrier opening [20].

We have already found that both the downward and upward frequency chirps could significantly reduce the grating lobe and the subsequent pre-focal heating, especially at the large axial focus shifting distance, as confirmed in both simulation and experiment [21]. Meanwhile, HIFU ablation ability in the main lobe was even enhanced. In order to understand the mechanism of lesion enhancement, the frequency chirps were further investigated extensively here. Numerical simulation was first performed to compare the acoustic field and subsequently, the bubble dynamics and temperature elevation using different excitations (the constant frequency excitation, downward and upward frequency chirps). Paramount parameters of the frequency chirps (e.g., the sweeping direction, frequency range, and time) were then examined for the optimal outcome. Lesion formation, bubble cavitation, and temperature rise induced by HIFU exposure were studied in the tissue-mimicking phantom and *ex vivo* porcine muscle and kidney samples. Lesion formation in the transparent polyacrylamide gel phantom was captured by a camcorder; bubble cavitation activities were monitored by passive cavitation detection (PCD), and temperature rise in the focal region was measured by a fine needle thermocouple. The produced lesions in the exercised porcine kidney samples were also compared with each other. Altogether, it is found that although there are no significant differences in the simulated distribution of average pressure in the axial and lateral directions, the enhanced cavitation by the frequency chirps could significantly increase the heating rate for the lesion production.

## 2. Material and method

### 2.1. HIFU transducer and frequency sweeping

An annular focused HIFU transducer (H-102G, outer diameter = 69.94 mm, inner diameter = 22.0 mm, $F$ = 62.64 mm, Sonic Concepts, Woodinville, WA) working at its third harmonic frequency, 3.3 MHz, was used in both numerical and experimental investigation. Its −6 dB bandwidth is about 0.8 MHz (2.9–3.7 MHz). Paramount parameters of the linear frequency sweeping (e.g., the frequency sweeping directions, range, and time) were investigated. Excitation at the constant frequency, 3.3 MHz, was used for comparison. There were 3 frequency sweeping ranges (e.g., 0.2 MHz, 0.3 MHz, and 0.4 MHz corresponding to 3.2–3.4 MHz, 3.15–3.45 MHz, and 3.1–3.5 MHz, respectively) which are all within −1 dB bandwidth of the HIFU transducer according to the specification provided by the manufacturer for the similar acoustic output, 3 different sweeping times (e.g., every 1 ms, 10 ms, and 100 ms), and two sweeping directions (upward or downward). These sweeping times were selected because of the pulse duration on the order of ms in clinical HIFU ablation, and the frequency chirps will be repeated if the pulse duration is longer than the sweeping time.

### 2.2. Numerical simulation

The nonlinear acoustic wave propagation and waveform distortion generated by the HIFU transducer were simulated by the Khokhlov-Zaboltskaya-Kuznetsov (KZK) equation using HIFU Simulator (Food and Drug Administration, Silver Spring, MD) [22].

$$\frac{\partial p}{\partial z}-\frac{\beta}{c_0^3\rho_0}p\frac{\partial p}{\partial \tau}-\frac{b}{2c_0^3}\frac{\partial^2 p}{\partial \tau^2}=\frac{c_0}{2}\int_{-\infty}^{\tau}\Delta_{\perp}p(\tau')d\tau' \tag{1}$$

where $p$ is the acoustic pressure, $z$ is the coordinate along the beam axis, $c_0$ is the small-signal sound speed, $\rho_0$ is the ambient density, $\tau = t-z/c_0$ is the retarded time, $\beta$ is the coefficient of nonlinearity, $b$ is the dissipative parameter, and $\Delta_{\perp}$ is the Laplacian operator with transverse coordinates. In the frequency-domain schemes, the solution is represented in the form of a Fourier series expansion,

$$p(z, r, t)=\sum_{n=-\infty}^{\infty}C_n(z, r)\exp(-in\omega_0\tau) \tag{2}$$

where $\omega_0$ is the driving frequency of the HIFU pulses and $C_n$ is the complex amplitude of the $n$th harmonic.

The radial oscillation of a single spherical bubble coupled with zeroth-order gas diffusion in the acoustic field is described by the original Gilmore model [23].

$$R\left(1-\frac{U}{C}\right)\frac{dU}{dt}+\frac{3}{2}\left(1-\frac{U}{3C}\right)U^2=\left(1+\frac{U}{C}\right)H+\frac{1}{C}\left(1-\frac{U}{C}\right)R\frac{dH}{dt} \tag{3}$$

where $R$ is the bubble radius, $U = dR/dt$ is the velocity of the bubble wall, and $C$ and $H$ Hare the speed of sound in water at the bubble wall and the enthalpy difference between the liquid at pressure $P(R)$ and pressure $P_\infty = P_0 + P_S$, respectively. $P_0$ is the ambient pressure of the surrounding liquid, and $P_S$ is the acoustic driving pressure. The Tait state Hequation for a compressible fluid and the pressure at the bubble wall $P(R)$ are described as following,

$$P = A(\rho/\rho_0)^m-B \tag{4}$$

$$P(R) = P_g - \frac{2\sigma}{R} - \frac{4\mu}{R}U \tag{5}$$

where $P_g$ is the gas pressure inside the bubble, $\mu$ and $\sigma$ are the viscosity and surface tension of the liquid, $A = c_0^2\rho/P_0 m$, $B = A-1$, and $m = 7$. The number of gas moles inside a bubble is determined by the zeroth-order solution to the diffusion equation [24],

$$n = n_0 - 4\sqrt{\pi D}\int_0^\tau F(\tau')(\tau-\tau')^{-1/2}d\tau' \tag{6}$$

where $D$ is the gas diffusion constant in the liquid, $n_0$ is the initial number of gas moles.

$$\tau = \int_0^t R^4(t')dt' \tag{7}$$

$$F(\tau) = C_0(P_g/P_0) - C_i \tag{8}$$

$$P_g = \left(P_0 + \frac{2\sigma}{R_0}\right)\frac{n}{n_0}\left(\frac{R_0}{R}\right)^{3\eta}\left(\frac{R_{0n}}{R_0}\right)^{3(\eta-1)} \tag{9}$$

where $R_0$ is the initial bubble radius, $R_{0n}(t)$ is the time-varying equilibrium bubble radius, $\eta$ is the polytropic exponent of the gas, $C_0$ and $C_i$ are the saturated and initial gas concentration in the liquid, respectively.

The BioHeat transfer equation was used to calculate the HIFU-induced temperatures, $T$, in the medium [25],

$$\rho_0 C_v\frac{\partial T}{\partial t} = \kappa\Delta T - h(T-T_0) + Q \tag{10}$$

where $C_v$ is the heat capacity, $\kappa$ is the thermal conductivity, $h$ is the convective heat transfer coefficient, $T_0$ is the equilibrium temperature and $\Delta$ is the Laplacian operator. The absorbed acoustic energy as a heat source, $Q$, is given by

$$Q = 4\sum_{n=0}^{20}\alpha_n|C_n|^2/c_0\rho_0 \tag{11}$$

where $\alpha_n = \alpha_0(nf)^a$ is the attenuation coefficient of the $n$-th harmonic in the pressure waveform. There are three types of energy depositions and conversion into heat from the dynamics of microbubbles in an acoustic field: $W_{th}$ is the heat deposition and conduction between the gas and the liquid; $W_{vis}$ is the viscous dissipation near the boundary of the bubble; $W_{ac}$ is the acoustic emission from the oscillating at the interface [26].

$$W_{th} = -\kappa\frac{\partial T}{\partial r}\cdot 4\pi R^2,\quad W_{vis} = 4\mu\frac{\dot{R}}{R}\cdot\dot{R}\cdot 4\pi R^2,\quad W_{ac} = \frac{\rho}{c_0}(R\ddot{R} + 2\dot{R}^2)^2\cdot 4\pi R^2 \tag{12}$$

The computation domain has two subdomains: water (3 cm from the aperture), and either tissue or phantom. Parameters used in the simulation are from the literature (Connor and Hynynen, 2002; Hallaj et al., 2001; Khokhlova et al., 2006) and listed in Table 1. The initial acoustic pressure was set as 250 kPa, and the lateral and axial step sizes were 0.02 mm and 0.035 mm, respectively, which are chosen to achieve the acoustic pressure at the focus comparable to that in the clinical HIFU ablation in the sufficient simulation resolution. The envelope of the pressure waveform at the focus, and the average peak positive and negative pressure distributions along and transverse to the transducer axis at three different excitation strategies (constant frequency at 3.3 MHz, upward and downward frequency sweeping in the range from 3.1 MHz to 3.5 MHz in 100 μs) are compared. Eq. (3) was solved by using the fifth-order Runge-Kutta-Fehlberg method with a step-size control algorithm [27]. All simulations were carried out on a 64-bit personal computer (Precision WorkStation T7610, Dell, Austin, TX) with Intel(R) Xeon(R) CPU E5-2630 v2 2.60 GHz processors and 64 GB of RAM.

**Table 1**
Material properties used in the simulation.

| Properties | Water | Phantom | Tissue |
|---|---|---|---|
| Nonlinear coefficient ($B/A$) | 3.5 | 5 | 7 |
| Attenuation coefficient ($\alpha_0$, dB/cm/MHz$^a$) | 0.0022 | 0.15 | 0.54 |
| Power of attenuation ($a$) | 2 | 1 | 1 |
| Sound speed ($c$, m/s) | 1500 | 1544 | 1570 |
| Density ($\rho$, kg/m$^3$) | 1000 | 1044 | 1080 |

### 2.3. Gel phantom and tissue preparation

The optically transparent polyacrylamide gel with 7% of bovine serum albumin (BSA) was prepared to study the HIFU-induced lesion and bubble activities [28]. The liquid mixture of polyacrylamide, BSA, and the Tris-Buffer was degassed for about 1 h in a desiccant chamber (420100000, Scienceware, Pequannock, NJ) by a vacuum pump (VTE8, Thomas, Sheboygan, WI) at a pressure of 150 mbars, then the degassed mixture was poured into a custom mold (L × W × H = 6 cm × 2.5 cm × 2.5 cm). The polymerization was finalized by the addition of 10% (w/v) ammonium persulfate solution (APS, Sigma-Aldrich, Singapore) and N,N,N′,N′-tetra-methylethylene/diamine (TEMED, Sigma-Aldrich).

Porcine muscles and kidneys were purchased from a commercial food market and then cut into the similar size (3 cm × 3 cm × 2 cm). The surfaces were carefully peeled to provide a smooth water–tissue interface. All tissue samples were first immersed in the phosphate-buffered saline (PBS) and degassed for approximately 1 h before the experiments.

### 2.4. Experimental setup

The input signals produced by the function generator were amplified by a power amplifier (BT00250-AlphaA, Tomco Technologies, Adelaide, Australia) before delivering to the matching unit and the HIFU transducer. Both the HIFU transducer and the phantom or *ex vivo* samples were immersed in the degassed and deionized water ($O_2$ < 4 mg/L, $T$ = 25 °C, measured by DO700, Extech Instrument, Waltham, MA) of a Lucite tank ($L \times W \times H$ = 70 cm × 50 cm × 30 cm). A silicone rubber acoustic absorber was put in the tank to minimize the ultrasound reflection. A three-axis positioning stage (BiSlide, Velmex, Bloomfield, NY) was employed to align the HIFU focus to the desired position (see Fig. 1). A LabView program (National Instruments, Austin, TX) was written to control the HIFU exposures (pulse repetition frequency of 1 Hz, duty cycle of 10%, pulse duration of 100 ms, and total exposure of 50 s) with an *in-situ* pressure ($p^+$ = 33.1–42.3 MPa and $|p^-|$ = 7.9–9.0 MPa at the driving frequency of 3.1–3.5 MHz, see Fig. 2a) measured by a needle hydrophone (HNA-0400, Onda, Sunnyvale, CA) using the established acoustic field characterization protocol [29]. HIFU focus was aligned 1 cm below the surface of gel or *ex vivo* samples. Accurate alignment was achieved by first maximizing the amplitude of echo from the sample surface with a pulser/receiver (5072PR, Olympus-IMS, Waltham, MA) and then moving 1 cm forward by the translational stage. After each exposure, the HIFU focus was moved laterally by about 8 mm to another spot within the same sample to avoid the influence of the previously treated region.

### 2.5. Temperature measurement

A 0.5 mm diameter thermocouple (TJ36-ICSS-020G-6, Omega Engineering, Stamford, CT) was inserted into the sample and was aligned perpendicular to the HIFU transducer axis to measure the temperature rise. The measured temperature elevations by a data acquisition (DAQ) unit (NI-9214, National Instruments) at a sample rate of 200 Hz were transferred to a PC for processing and analysis in OriginPro (OriginLab, Northampton, MA). Due to the migration of the lesion location, the tip of the thermocouple was aligned 3 mm in front of the focus axially. The thermal couple was initially aligned to the

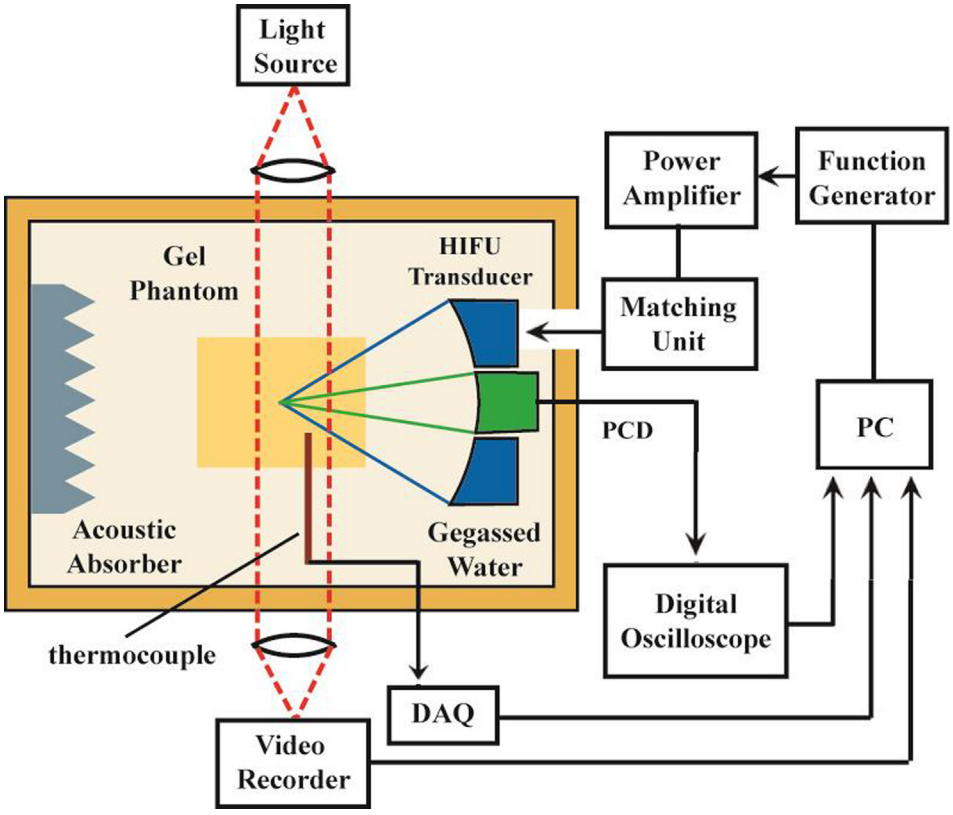


**Fig. 1.** Schematic diagram of the experimental setup. The HIFU transducer and passive cavitation detection (PCD) transducer were aligned confocally and coaxially.

HIFU focus by obtaining the maximum acoustic echo from the tip and then moved to the desired position by the translational stage.

### 2.6. Lesion detection

A 100 W white-light bulb under the water tank provided the illumination source through the gel phantom for the photography. The lesion formation process in the transparent gel phantom was recorded by a digital video camera (Vixia HF M500, Canon, Tokyo, Japan) at a frame rate of 50 Hz and a shutter speed of 1/2000 s. The video data were imported into the FreeStudio (V6.3, DVDVideoSoft, UK) to extract the images and then process them by the ImageJ software (National Institutes of Health, Bethesda, MD). The lesion boundary detection was accomplished using the edge detection function, and the lesion area was determined after calibrating the resolution with a ruler. After the HIFU exposure, the lesions in both the side view and top view were recorded photographically by a digital camera (PowerShot SX230 HS, Canon), and the photos were processed in the same way.

### 2.7. Bubble cavitation measurement and analysis

Bubble activities only during the HIFU exposure (those during the burst interval are ignored) were detected with a 15-MHz focused transducer (V313, $F = 65$ mm, $D = 12.7$ mm, Olympus-IMS) by aligning it confocally and coaxially to the HIFU transducer for PCD, and the cavitation signals were acquired by a digital oscilloscope (Wavesurfer MXs-B, LeCroy, Chestnut Ridge, NY) at a sampling frequency of 50 MHz in the sequence mode and finally transferred to a PC for data analysis using the short-time Fourier transforms (STFT, 2048-points, zero overlapping window) [30] in the MatLab (The MathWorks, Natick, MA). The STFT spectrum went through a notch comb filter to remove the harmonic, ultra-harmonic, and super-harmonic components, and then the root mean square (RMS) value during each HIFU pulse was used to quantify the IC level [31]. For the scattering level, a 200 kHz bandpass filter was applied to the STFT spectrum around the third harmonic. Due to a large amount of data involved and limited memory of the oscilloscope, PCD signals were collected every 5 pulses. During each sonication period, the PCD data, temperature rise, and video recording were simultaneously collected and synchronized with HIFU exposure.

### 2.8. Statistical analysis

At each experimental condition, at least eight data were collected, from which the mean value and standard deviation were performed. Analysis of variance (ANOVA) was performed in SPSS® Statistics (IBM Software, Somers, NY) to determine the statistical difference between testing groups that was fixed at the confidence value of $p < 0.05$.

## 3. Results

### 3.1. Simulation of acoustic and thermal field

The simulated acoustic pressure waveforms at the HIFU focus in the gel phantom show significant distortion (much larger peak positive pressure than peak negative one) due to the generation of high order harmonics during the nonlinear acoustic propagation (see Fig. 2a). At the linear frequency sweeping, the changes in the peak positive pressure are much larger than that in the peak negative pressure (see Fig. 2b). The high pressure at the high frequency is due to the increased focusing gain, $G = \omega_0 a_f^2/2c_0/d_f$ where $\omega_0$ is the angular frequency, $a_f$ is aperture radius, $d_f$ is the distance between the aperture and the focal plane. Average pressure distributions in the axial and lateral direction at the constant frequency of 3.3 MHz and frequency sweeping in the range of 3.1–3.5 MHz in the tissue are shown in Fig. 2c and d, respectively. The characteristics of the acoustic field in water, gel phantom, and tissue are listed in Table 2. The average magnitude and distribution of acoustic pressure of the frequency chirps are similar to those of the

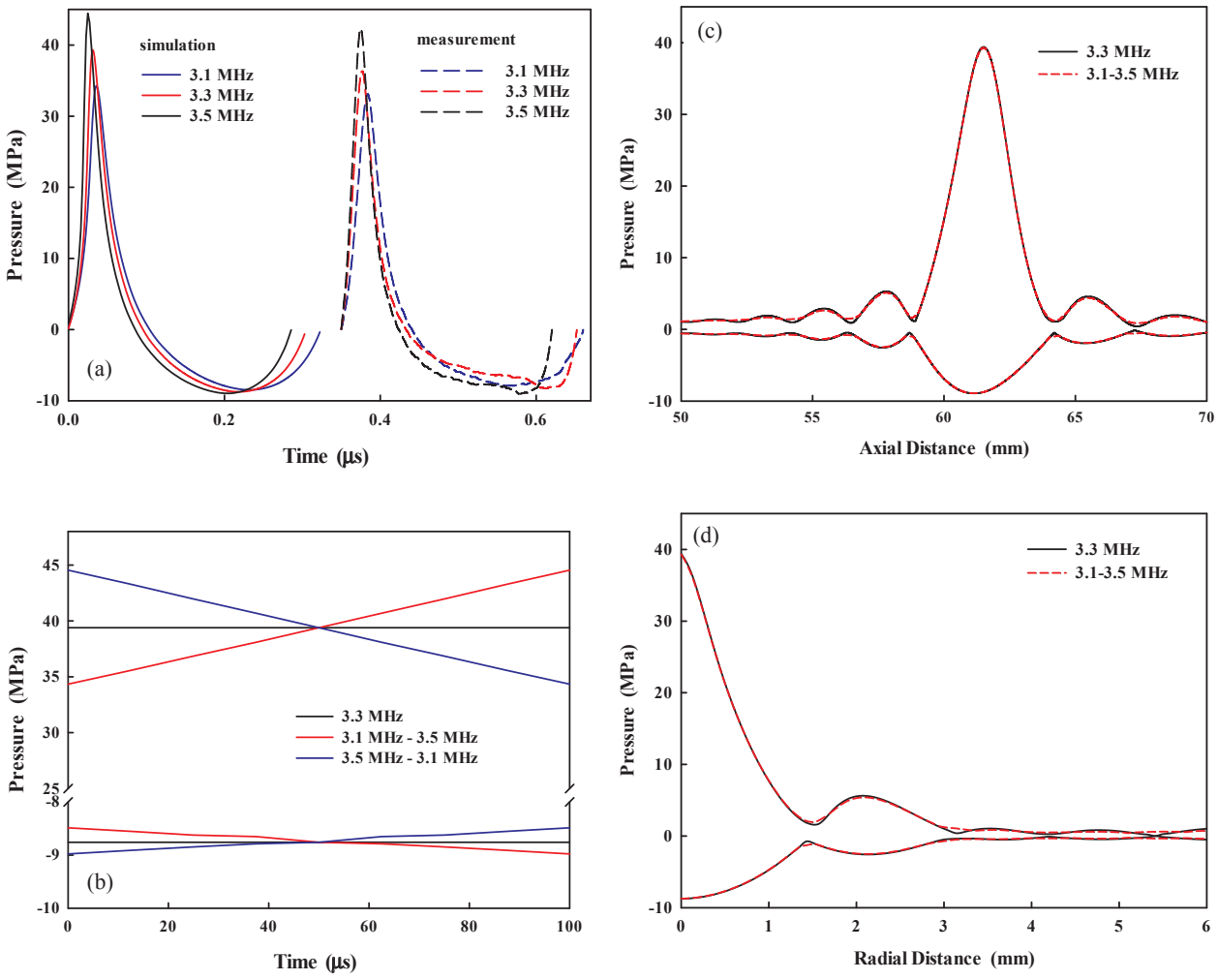


**Fig. 2.** Comparison of the (a) pressure waveforms at the focus at the frequency of 3.1 MHz, 3.3 MHz, and 3.5 MHz (simulation in solid line and measurement in dashed line with the retarded time of 0.35 μs), (b) envelope of HIFU pressure waveform at the focus at the constant frequency of 3.3 MHz, upward frequency chirp from 3.1 MHz to 3.5 MHz, and downward frequency chirp from 3.5 MHz to 3.1 MHz, simulated axial (c) and lateral (d) average pressure distribution in the gel phantom using different excitations.

**Table 2**
Peak positive and negative pressure obtained in the simulation.

| | | Water | Gel phantom | Tissue |
|---|---|---|---|---|
| Average peak positive pressure (MPa) | Constant | 41.57 | 39.39 | 22.36 |
| | Sweep | 41.54 | 39.31 | 21.82 |
| Average peak negative pressure (MPa) | Constant | −8.93 | −8.76 | −6.05 |
| | Sweep | −8.91 | −8.74 | −6.07 |
| −6 dB beam size of peak positive pressure (mm × mm) | Constant | 4.76 × 0.49 | 4.76 × 0.50 | 4.76 × 0.55 |
| | Sweep | 4.76 × 0.49 | 4.76 × 0.50 | 4.76 × 0.55 |
| −6 dB beam size of peak negative pressure (mm × mm) | Constant | 7.50 × 1.02 | 7.49 × 1.04 | 7.49 × 1.10 |
| | Sweep | 7.59 × 1.02 | 7.58 × 1.04 | 7.58 × 1.10 |

constant frequency excitation although the magnitudes at the pressure nodes whose locations are highly dependent on the driving frequency are slightly larger (e.g., 0.4 MPa). The sweeping direction and rate have little influence on the acoustic field, and the −6 dB beam sizes (axial × lateral) are similar. The other frequency sweeping ranges of 0.2 MHz and 0.3 MHz were not included, but with the same conclusions (almost identical average peak pressure and beam size, but discrepancies at the pressure nodes becoming significant with the frequency sweeping range).

The bubble dynamics induced by different excitations are shown in Fig. 3a–c. It is found that frequency chirps could enhance the bubble dynamics, and the maximum and average bubble radius expansion over 100 μs at the upward or downward frequency sweeping are 8.97 fold and 4.51 fold, and 8.42 fold and 4.71 fold, respectively. In comparison, the corresponding values at the constant frequency are 7.9 fold and 4.47 fold. The temperature elevations by 100 μs-HIFU exposure using these three excitations (constant at 3.1 MHz, 3.3 MHz, 3.5 MHz, 3.1–3.5 MHz upward, 3.5–3.1 MHz downward frequency sweeping) are 0.3198 °C, 0.3334 °C, 0.3524 °C, 0.3466 °C, and 0.3457 °C, respectively. The difference may be due to the high amplitudes of harmonics at the high frequency. With the inclusion of bubble-enhanced heating, the corresponding values are 0.3583 °C, 0.3606 °C, 0.3691 °C, 0.3703 °C,

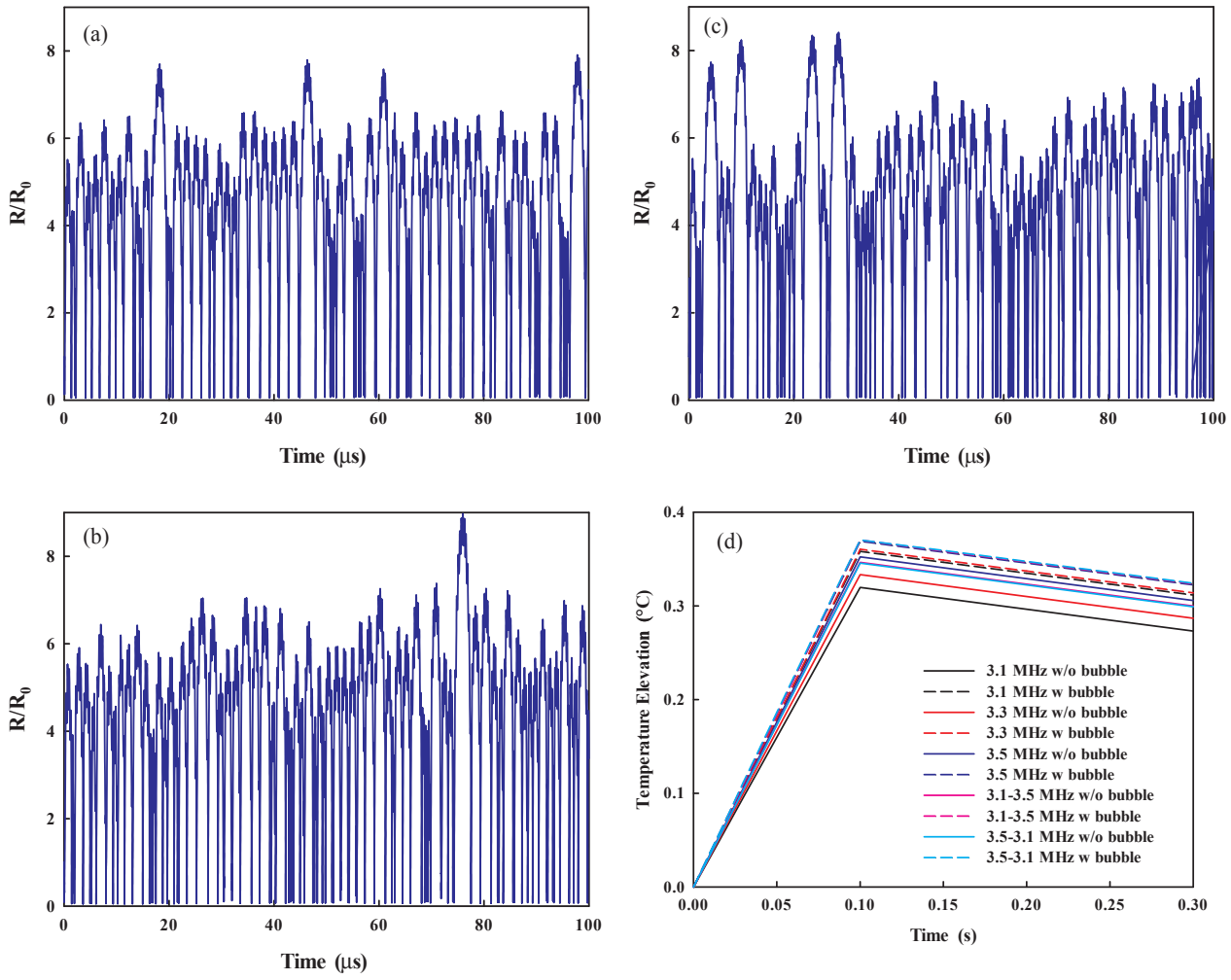


**Fig. 3.** The simulated dynamics of bubble at the initial radius of 3 μm by 100 μs-HIFU exposure (a) at the constant frequency of 3.3 MHz, (b) at the downward and (c) upward frequency chirps in the frequency sweeping range from 3.1 MHz to 3.5 MHz in water, and (d) the temperature elevations by these excitation strategies followed by 200 μs relaxation time without (solid line) and with (dashed line) inclusion of bubble-enhanced heating in the gel phantom.

**Table 3**
Bubble expansion and cavitation-induced temperature rise for 100 μs-HIFU ablation by different excitation strategies.

| $f$ (MHz) | $R_0$ (μm) | $R_{max}/R_0$ | $\overline{R}/R_0$ | $\Delta T$ (°C) |
|---|---|---|---|---|
| 3.1 | 1 | 27.63 | 14.07 | 0.0397 |
| 3.3 | 1 | 24.11 | 13.42 | 0.0419 |
| 3.5 | 1 | 21.97 | 13.05 | 0.0472 |
| 3.1–3.5 | 1 | 26.50 | 13.65 | 0.0434 |
| 3.5–3.1 | 1 | 25.90 | 14.20 | 0.0469 |
| 3.1 | 3 | 9.42 | 4.93 | 0.3583 |
| 3.3 | 3 | 7.90 | 4.47 | 0.3606 |
| 3.5 | 3 | 6.68 | 4.16 | 0.3691 |
| 3.1–3.5 | 3 | 8.97 | 4.51 | 0.3703 |
| 3.5–3.1 | 3 | 8.42 | 4.71 | 0.3705 |
| 3.1 | 5 | 5.78 | 2.95 | 0.8093 |
| 3.3 | 5 | 3.95 | 2.68 | 0.8478 |
| 3.5 | 5 | 3.06 | 2.41 | 0.9357 |
| 3.1–3.5 | 5 | 5.33 | 2.74 | 0.8862 |
| 3.5–3.1 | 5 | 5.09 | 2.87 | 0.9723 |

and 0.3705 °C, respectively (see Fig. 3d). Simulation data are listed in Table 3. Overall, it suggests that HIFU ablation using the frequency chirps could generate higher temperatures in comparison to that at the constant frequency. Although short HIFU exposure was used in the simulation (100 μs) because of the very high computation burden, the discrepancies between different excitations will become more significant in long clinical HIFU ablation.

### 3.2. Temperature measurement in the gel phantom

The temperature rises measured by the thermocouple using the frequency chirps (at different sweeping ranges and times) and constant frequency excitations in the gel phantom are compared in Fig. 4. Large variations may be due to the alignment error of the thermocouple and the displacement and deformation of the gel phantom by the acoustic radiation force during HIFU exposure. The conventional HIFU excitation at the constant frequency always had the lowest temperature rises. There are no significant differences between the downward and upward frequency chirps ($p > 0.05$) while in most of the cases the downward frequency chirp had slightly higher temperatures. Increasing the frequency sweeping range or decreasing the sweeping time led to higher temperature rises (e.g., 61.1 ± 1.7 °C and 59.2 ± 1.6 °C for the downward and upward frequency chirp at the frequency sweeping range of 0.4 MHz in 1 ms, respectively).

### 3.3. Lesions in the gel phantom

At the beginning of HIFU ablation, a small cigar-shaped lesion was formed at the focus due to the absorption of the incident ultrasound wave. Then the lesion gradually became tadpole-shaped and migrated

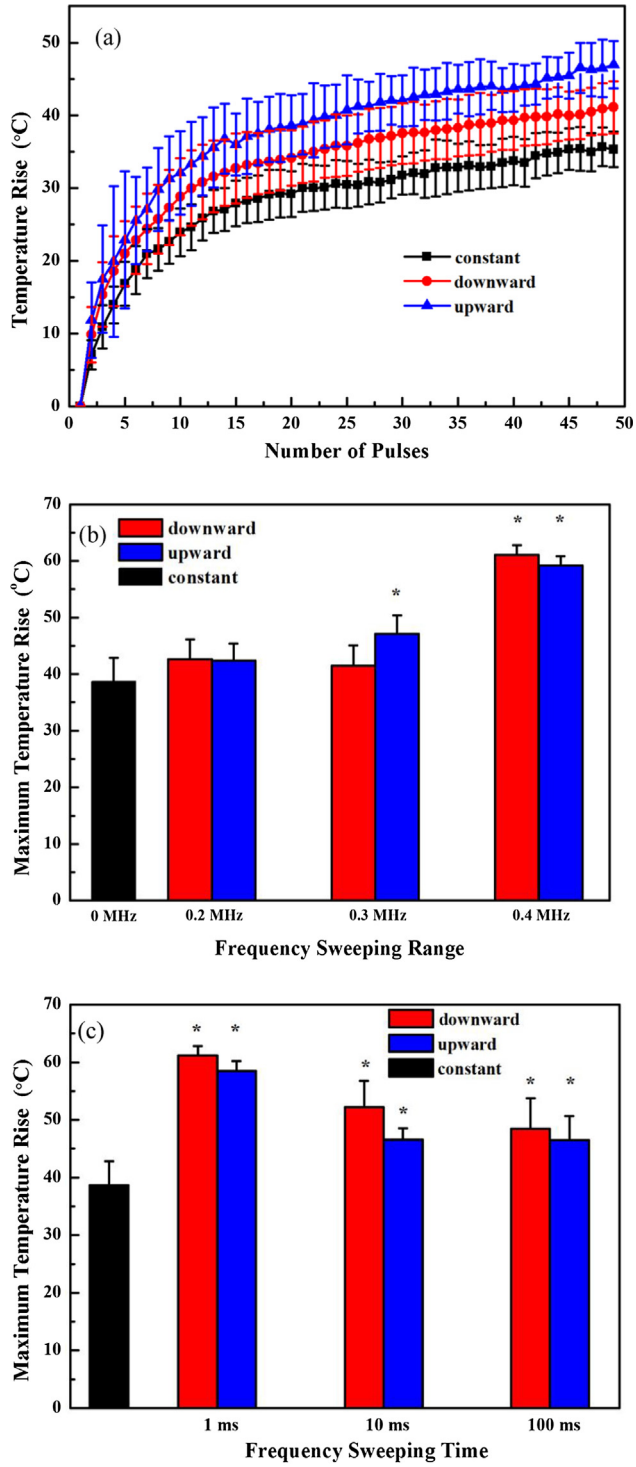


**Fig. 4.** (a) The temperature rise at the focal point measured in the gel phantom at the frequency sweeping range of 0.3 MHz, and comparison of the maximum temperature rise at the varied (b) frequency sweeping ranges and (c) times at the end of 50 HIFU pulses (*: $p < 0.05$ in comparison to those lesion generation at the constant frequency).

toward the transducer. So the progressive changes in the lesion area from the side view were monitored and compared from the 15th HIFU pulse (see Fig. 5). It is shown that produced lesions using the frequency chirps were statistically larger than those using the constant frequency at all testing parameters ($p < 0.05$). Although there is no significant difference between two frequency chirps ($p > 0.05$), the downward frequency chirps seem slightly better than the upward ones. With the proper selection of frequency sweeping parameters (e.g., frequency sweeping range of 0.4 MHz and sweeping time of 1 ms), lesion enlargement as large as 50% could be achieved.

The lesions produced in the BSA polyacrylamide gel phantom by different excitation strategies are shown in Fig. 6. It's clear that using both the downward and upward frequency chirps could produce larger tadpole-shaped lesions than those using the constant frequency, which may be due to the enhanced acoustic cavitation. The quantitative lesion areas in both the side view and top view produced by different excitations are shown in Fig. 7. As the frequency sweeping range increased from 0.2 MHz to 0.4 MHz, the lesion area enlargement gradually increased from 35.1% to 50.0% in the side view and from 32.8% to 49.1% in the top view, respectively, using the downward frequency chirp. In comparison, lesion enhancement using the upward frequency sweeping is slightly lower. Corresponding enlargements are from 23.7% to 44.6% in the side view and from 23.2% to 44.6% in the top view, respectively. However, with the increase of the sweeping time from 1 ms to 100 ms, the lesion size enlargement only drops slightly in the side view (from 50.4% to 37.8% in the downward frequency chirp and from 44.6% to 37.4% in the upward frequency chirp, respectively) while much fewer changes in the top view (from 49.1% to 45.9% in the downward frequency chirp and from 44.6% to 45.1% in the upward frequency chirp, respectively). Overall, the frequency sweeping range has a greater impact in the gel phantom.

### 3.4. Bubble cavitation in the gel phantom

To figure out the underlying mechanism for the enlarged lesion size with the frequency chirp excitations, bubble cavitation during HIFU exposures were monitored by PCD. Representative 100-ms PCD signals with the corresponding spectra are shown in Fig. 8. After the FFT, the discrete spectra were found at the fundamental frequency (3.3 MHz) and high harmonics (e.g., 6.6, 9.9, 13.2 MHz) by the constant frequency excitation (see Fig. 8b). In contrast, the spectra of frequency chirps spread in a range which is proportional to the number of harmonic and frequency sweeping range (e.g., the 3rd harmonic spreading in the range from about 9.3 MHz to 10.5 MHz at the frequency sweeping range of 0.4 MHz). In addition, the spectra between harmonics were also high. In the STFT spectra, the sweeping direction could be observed clearly (see the boxes in Fig. 8c). In both spectra obtained using the FFT and STFT, few sub-harmonics ($f_0/2$, e.g., 1.55–1.75 MHz) or ultra-harmonics ($nf_0/2$) was found, which suggests that the stable cavitation does not dominate in the high power ablation and is similar to the findings in the previous studies [32,33]. The fundamental and harmonics in the spectra are the scattering signals of the HIFU burst from the bubble so that the 3rd harmonic was quantified to evaluate the scattering level.

The effects of frequency sweeping range and time on the scattering and IC in the gel phantom with the ongoing of HIFU ablation are shown in Figs. 9 and 10, respectively. The large standard deviation may be due to the varied bubble distribution. The frequency chirps could produce higher scattering and IC than that at the constant frequency ($p < 0.05$). The difference of HIFU-induced bubble cavitation gradually became apparent with the increase of frequency sweeping range from 0.2 MHz to 0.4 MHz and the decrease of frequency sweeping time from 100 ms to 1 ms. The downward frequency chirp had slightly lower scattering but higher IC than the upward one despite no statistical differences between them ($p > 0.05$). Meanwhile, the differences in the scattering and IC levels between the frequency chirps and the constant frequency excitation became larger with the ongoing of HIFU exposure. At the end of HIFU exposure, the differences in scattering and IC increased from about 3.4 dB to 6.4 dB and from 1.0 dB to 4.0 dB, respectively, at the frequency sweeping range from 0.2 MHz to 0.4 MHz. The corresponding values decreased from about 6.4 dB to 0.7 dB and from 1 dB to 0.02 dB, respectively, at the sweeping time from 1 ms to 100 ms.

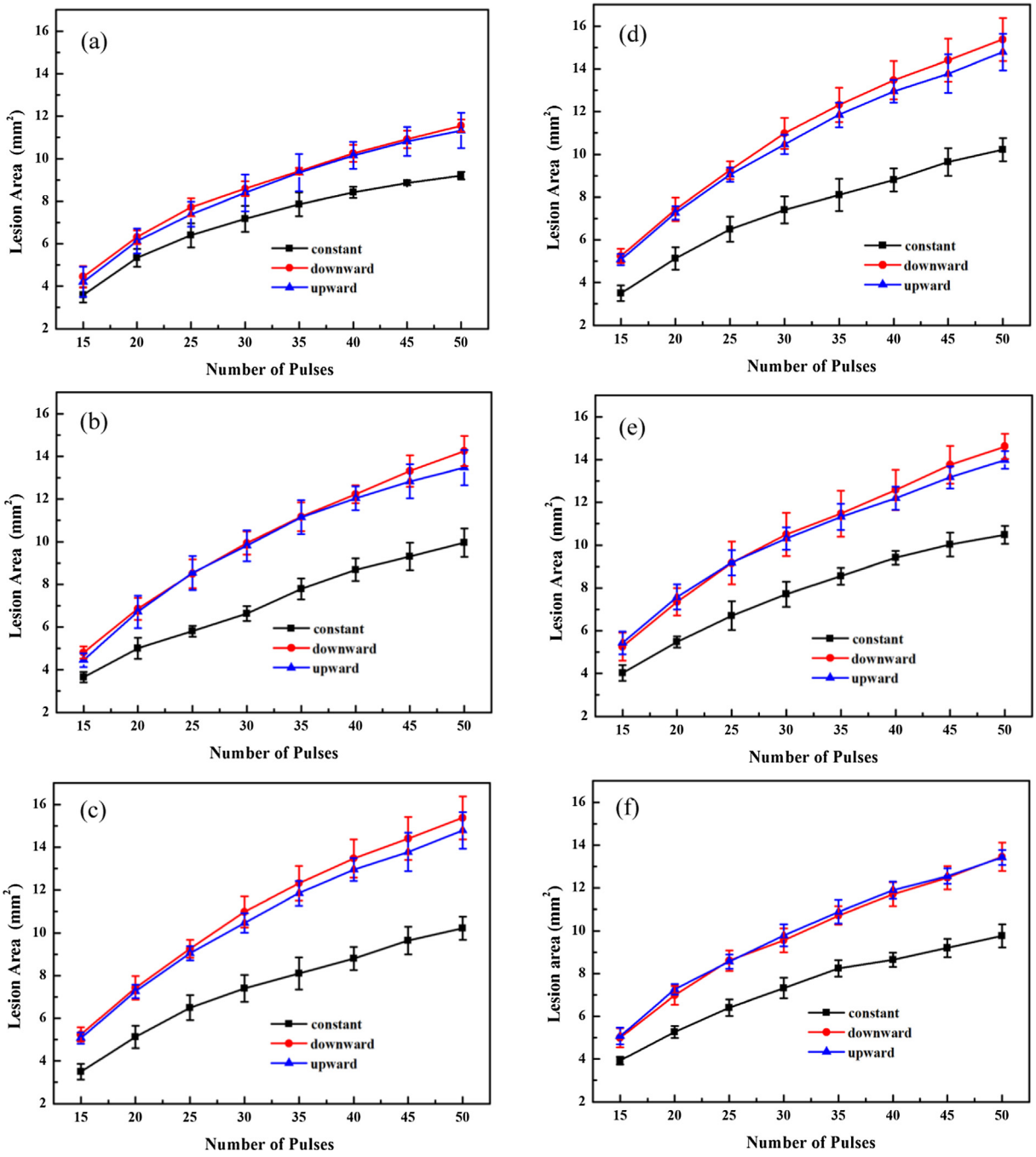


**Fig. 5.** Progressive lesion formation (side view) with the various frequency sweeping range of (a) 0.2 MHz, (b) 0.3 MHz, (c) 0.4 MHz in 1 ms, and frequency sweeping time of (d) 1 ms, (e) 10 ms, and (f) 100 ms at the frequency sweeping range of 0.4 MHz.

### *3.5. Temperature measurement in the ex vivo samples*

The effects of frequency sweeping range and time on the temperature rises in the porcine muscles are shown in Fig. 11. The temperature rises in the tissue were lower with smaller variation in comparison to those in the gel phantom due to its higher acoustic attenuation, but the differences between the frequency chirps and the constant frequency excitation were more significant, especially with the increase of the frequency sweeping range from 0.2 MHz to 0.4 MHz and decrease of the sweeping time from 100 ms to 1 ms. The downward frequency chirp was slightly better than the upward one despite no significance between them ($p > 0.05$). The artifacts associated with the thermocouple measurement, such as the viscous heating, heat conduction along the thermocouple, and the bubble shielding effect, may not be significant in both gel and tissue because of the low-temperature elevation, especially in the tissue. Thus, the major reason for the measurement error may be the alignment error of the ultrasound beam with respect to the thermocouple tip.

### *3.6. Lesions in the ex vivo samples*

The lesions produced in the porcine kidney samples after 1 min-HIFU ablation (the other parameters same as those used in the gel phantom) are shown in Fig. 12 with the frequency sweeping range and time of 0.4 MHz and 1 ms, respectively. Lesion areas in the axial direction produced by the downward and upward frequency chirps were significantly larger than that by the constant frequency excitation ($9.4 \pm 1.5\,mm^2$ and $9.0 \pm 1.0\,mm^2$ vs. $7.2 \pm 1.4\,mm^2$, $p < 0.05$).

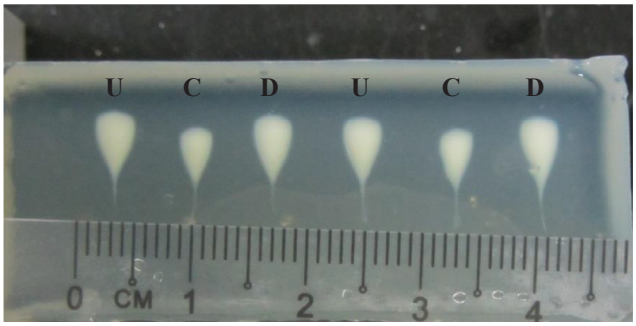


**Fig. 6.** Representative side view photograph of the lesions created by different excitations in the gel phantom (U: upward frequency chirp, C: constant frequency excitation, and D: downward frequency chirp).

The porcine kidney rather than muscle samples were used in the *ex vivo* lesion comparison because of higher image contrast for the easy boundary detection.

### 3.7. Bubble cavitation in the tissue

Variations of scattering and IC in the tissue at the different frequency sweeping ranges and times during HIFU exposure are shown in Figs. 13 and 14, respectively. Even though all samples were degassed for the same time, a large standard deviation was still retained due to the heterogeneity of *ex vivo* tissue and inconsistent bubble concentration remained in the samples. The differences in scattering and IC between the frequency chirps and the constant frequency excitation increased from 7.1 dB to 11.4 dB and from 0.01 dB to 2.4 dB, respectively, with the increase of frequency sweeping range. The frequency sweeping time seems to have a minor impact on the IC. The differences in the scattering among the excitations became smaller (from 11.4 dB to 5.4 dB) with the sweeping time increased from 1 ms to 100 ms. Overall, the frequency sweeping range plays a more important role than the sweeping time in the tissue. The changes on the IC in the tissue were much less than that in the gel phantom.

## 4. Discussion

HIFU ablation is sometimes limited by its low thermal deposition in highly perfused cancer/tumors. HIFU focus is scanned throughout the whole volume of a large target, which usually takes 1–2 h in clinics. The frequency chirps were found to enhance the ablation ability in the main lobe in our previous study [21], and such lesion enhancement was investigated extensively here. The simulated average pressure distributions by the constant frequency excitation and downward and upward frequency chirps are similar (difference < 2%) and have almost the same -6 dB beam size. However, HIFU-induced bubble dynamics and temperature elevations at these three excitations in the simulation suggest that bubble-enhanced heating may be the mechanism. Lesion enlargement increased and decreased with the frequency sweeping range and time, respectively, with a maximum enhancement of 50% in the gel phantom. PCD and thermocouples were utilized to monitor the process of HIFU ablation. It is found that scattering, inertial cavitation, and the consequent temperature rises are higher using the frequency

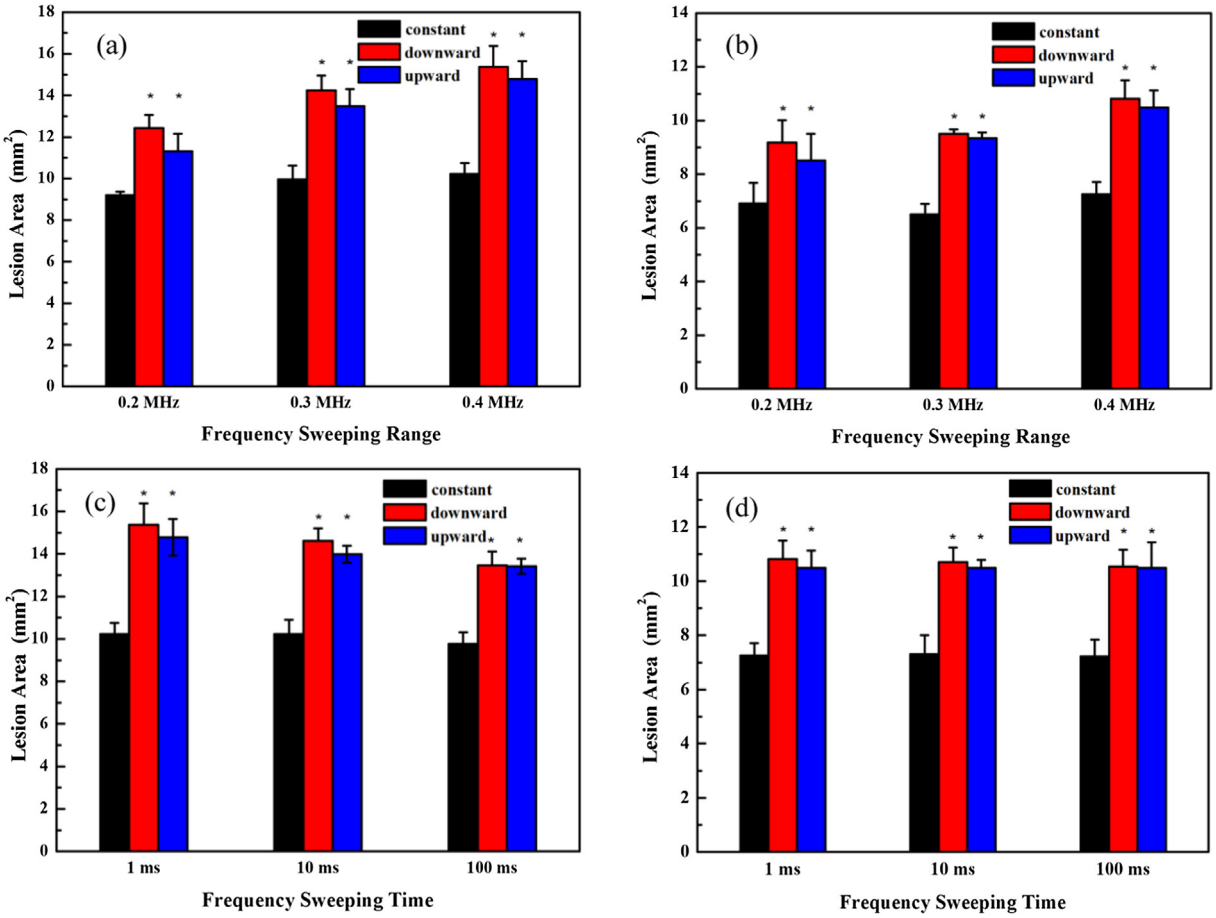


**Fig. 7.** Comparison of the lesion size generated by HIFU exposure in the (a) side view and (b) top view using the various frequency sweeping ranges from 0.2 MHz to 0.4 MHz in 1 ms, in the (c) side view and (d) top view using the various frequency sweeping times from 1 ms to 100 ms at the frequency range of 0.4 MHz (*: $p < 0.05$ in comparison to those lesion generation at the constant frequency).

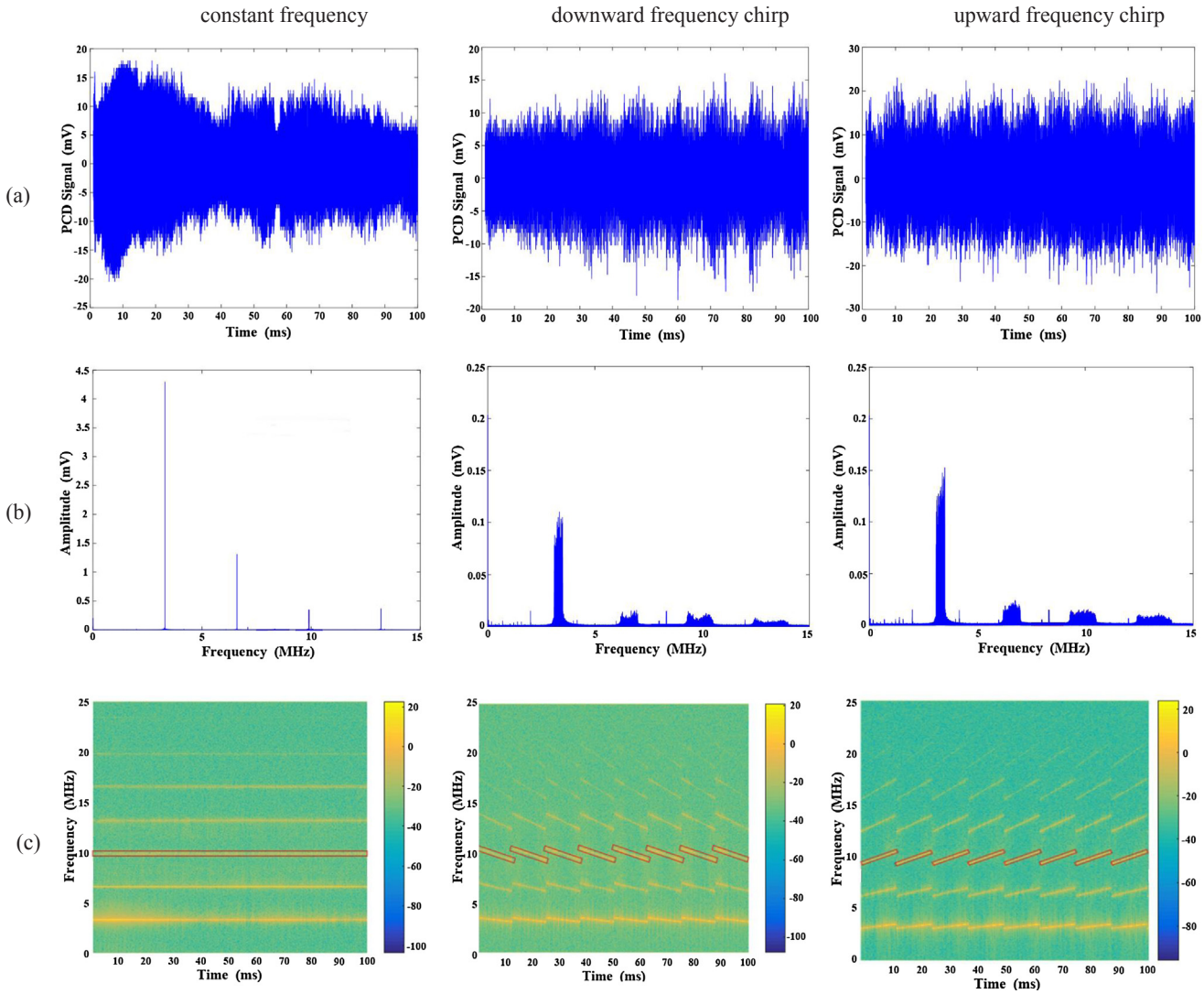


**Fig. 8.** (a) Passive cavitation detection (PCD) data, (b) the corresponding spectrum over the sonication time, and (c) the STFT spectrograms during one HIFU pulse at the pulse duration of 100 ms using the constant frequency excitation, downward frequency chirp, and upward frequency chirp, respectively, with the frequency sweeping range of 0.4 MHz in 10 ms. The color-bars in the STFT spectrograms represent the decibel (dB) value normalized to 1 mV. Boxes in the STFT spectrograms show the 3rd harmonic during the different excitations.

chirps in both gel phantom and *ex vivo* samples. All cavitation signals slightly increased with the exposure time. Overall, frequency chirps could effectively enhance the lesion production at the focus, and the enhancement is associated with the bubble cavitation. Short sweeping time and large frequency sweeping range are preferred.

There are several differences between the current study and the previous one which investigated the bubble activity in HIFU by the frequency chirps [19]. Firstly, this study was performed in the phantom and *ex vivo* tissue so that the bubble behavior is distinctively different due to the presence of viscosity and elasticity. The concentration of bubble nuclei in Luminol solution is higher than that in the gel phantom and tissue. And the solution was pre-sonicated for 2 min at 3.6 MHz to ensure the consistent population of bubble nuclei. Secondly, higher power (~150 W vs. 17 W) used in this study makes the drawn conclusions reasonable to be extrapolated to the clinical applications. Finally, a wide range of parameters (e.g., frequency sweeping range and sweeping time) were investigated, and their effects on the bubble cavitation and lesion enhancement were evaluated.

The role of cavitation in HIFU ablation is still under debate [10]. Above a certain threshold, the heating rate was significantly greater than that predicted by Eq. (11) without bubbles [9]. Enhanced acoustic cavitation by the frequency chirps may be due to several factors. The bubble may experience the resonance before growing to its maximum size followed by the collapse at a certain driving frequency. For a frequency chirp with broad spectra as shown in Fig. 8b, more cavitation activities of bubbles in a wide size distribution may be stimulated than that by a constant-frequency signal with discrete and narrow spectra [34]. Simulations and high-speed photography have shown increased bubble dynamics in response to chirp excitation [35]. It is well known that the thermal effect is more effective for high-frequency excitation while the mechanical effect is more predominant for the low-frequency one. In the downward frequency chirp, the high starting frequency will produce the high temperature initially which could be maintained in the gel phantom due to low thermal conduction and diffusion as shown in our thermocouple measurement. The raised temperature makes the sample air super-saturated, resulting in the air molecules dissolved unstable [17]. The vapor pressure and surface tension increases and decreases with the temperature, respectively. Therefore, the initially high temperature is beneficial for the occurrence of cavitation. In comparison, the initial low-frequency signal makes the bubble formation and expansion more prone due to the long duration of the tensile wave. Overall, the frequency sweeping direction, range, and time affect

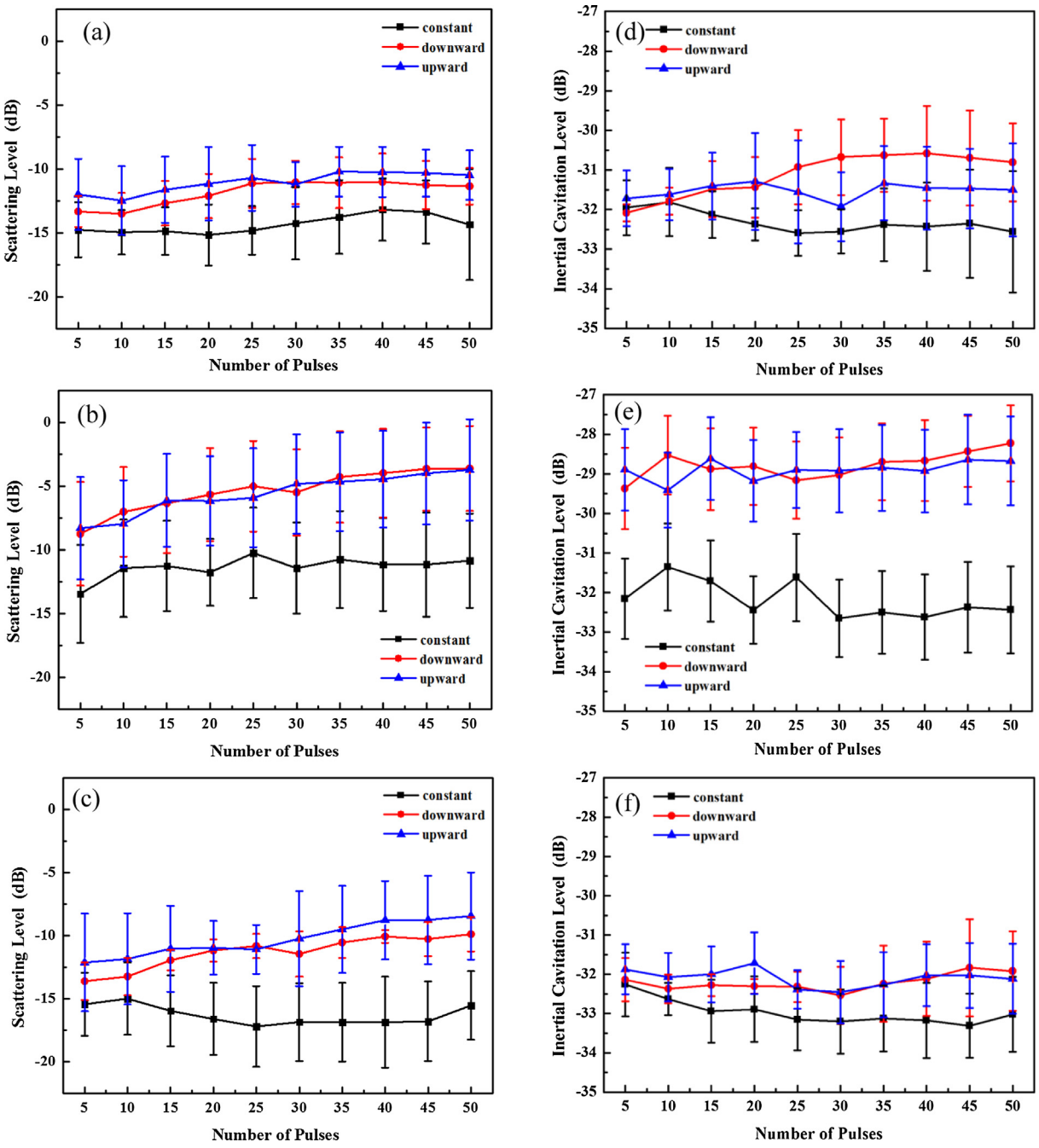


**Fig. 9.** The scattering level with the progress of HIFU exposure in the gel phantom with the frequency sweeping range of (a) 0.2 MHz, (b) 0.3 MHz, (c) 0.4 MHz in 1 ms, and the corresponding inertial cavitation levels from (d) to (f).

the growth and coalescence of bubbles. However, downward and upward sweeping have similar performance in the bubble cavitation and consequent lesion enhancement despite of different emphasis in the excitation. In comparison, a pseudorandom or broadband chirp excitation in water and Luminol solution decreased the sonochemiluminescence at the power of 40 W [36], which may be due to the absence of standing wave occurring from the cavitation at the focus. The sonochemiluminescence intensity and $I_3^-$ formation could be enhanced by 2 fold by a short downward frequency sweeping, but quenched in the upward direction [19]. In both studies, the temperature rises in the solution were ignored and acoustic intensities investigated were moderate, which may explain the discrepancy with our observations here. In addition, bubbles will backscatter the incident acoustic energy, which results in the bubble shielding effect and change of produced lesion from the symmetric shape of the cigar to the asymmetric shape of tadpole during HIFU ablation [9,37]. If a large boiling bubble is produced, such asymmetric lesion production will be more significant [38]. Initial bubble sizes of 1 μm and 5 μm were also included in the simulation and listed in Table 3. It is found that a smaller initial bubble has a larger bubble expansion ratio, but less cavitation-induced temperature elevation that is dependent on the bubble size according to Eq. (12). Such bubble size-dependent phenomenon is similar to sonoluminescence emission by pulsed ultrasound at the varied ultrasound power and frequencies [39]. Further investigation of the effect of frequency sweeping range and initial bubble size on the outcome is required to understand the underlying mechanism.

Although the high attenuation of tissue reduces the acoustic intensity at the HIFU focus, the low acoustic pressure is desirable for

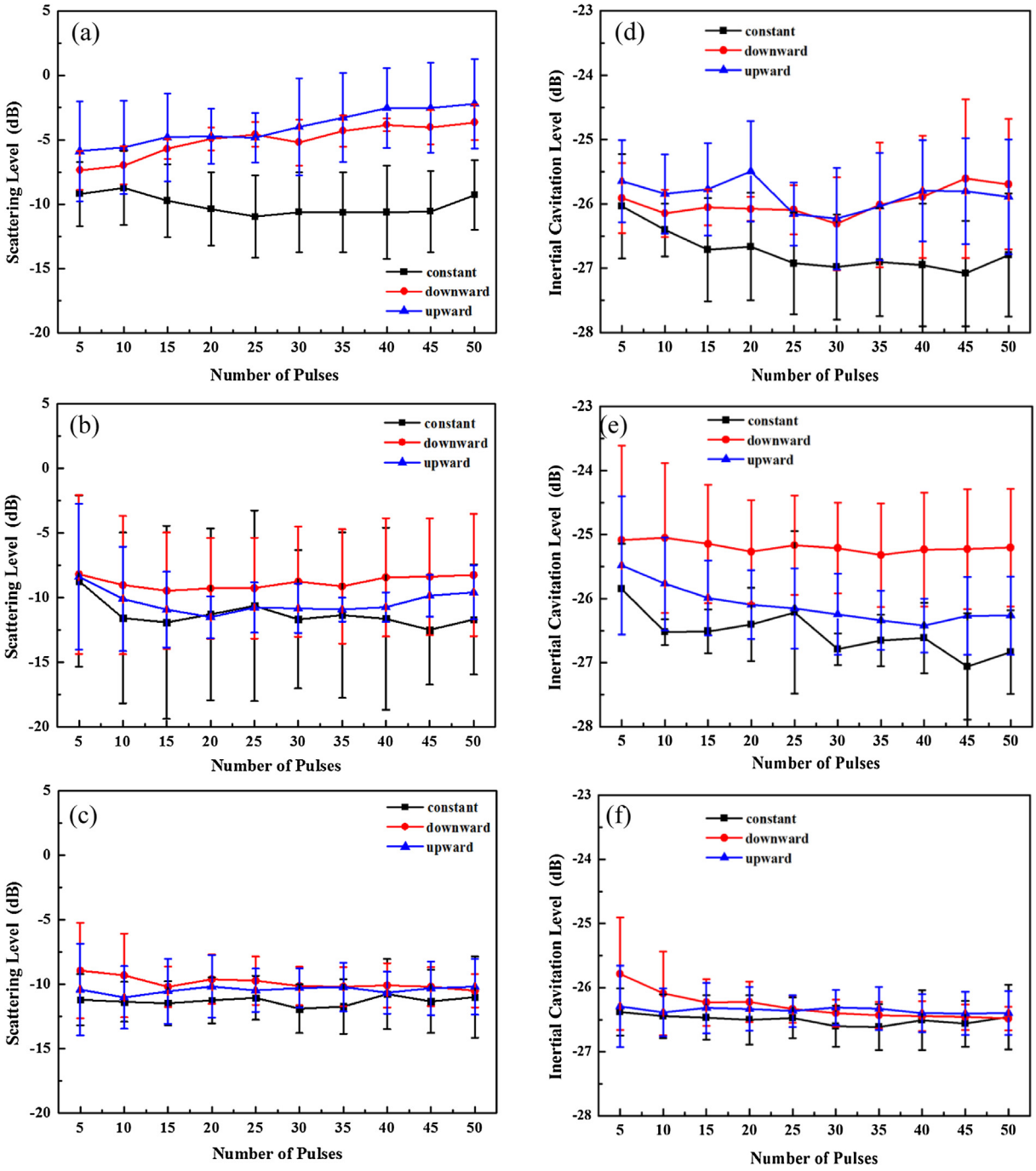


**Fig. 10.** The scattering level with the progress of HIFU exposure in the gel phantom with the frequency sweeping time of (a) 1 ms, (b) 10 ms, (c) 100 ms at the frequency sweeping range of 0.4 MHz, and the corresponding inertial cavitation levels from (d) to (f).

stable cavitation to facilitate the effective heating via the viscous loss at the temperature well below the boiling as the elevated vapor pressures serve to mitigate the violent collapse [10,40]. However, no significant stable cavitation associated sub-harmonic and ultra-harmonics were found in the spectra of our measured PCD data (e.g., continuous frequency sweep in the spectrogram as that of fundamental and harmonic components), which may be due to the quick bubble collapse induced by the large peak negative pressure. In the boiling regime, the dominant mechanism for the enhanced heating from the large vapor bubbles becomes the viscous boundary layer heating. However, no abrupt rise in the PCD signals was observed here so that HIFU-induced boiling may not occur [41]. With long HIFU ablation and the increase of ambient temperature, boiling may occur. The strong scattering of HIFU burst by a bubble cloud will trap acoustic energy within that region and produce greater absorption by viscous dissipation and thermal conduction [10]. Overall, the bubble-induced heating can be greater than the absorbed acoustic energy only. The temperature rise induced by cavitation was found correlate well with “cavitation power” so that monitoring HIFU ablation in real-time may be possible [42].

PCD has been used widely to monitor the cavitation activities during HIFU ablation. Several methods have been tried to quantify the bubble cavitation in this study (data not included). RMS values of PCD signals were used to evaluate the cavitation, but they cannot separate the roles of stable and inertial bubble cavitation. A combo band-pass

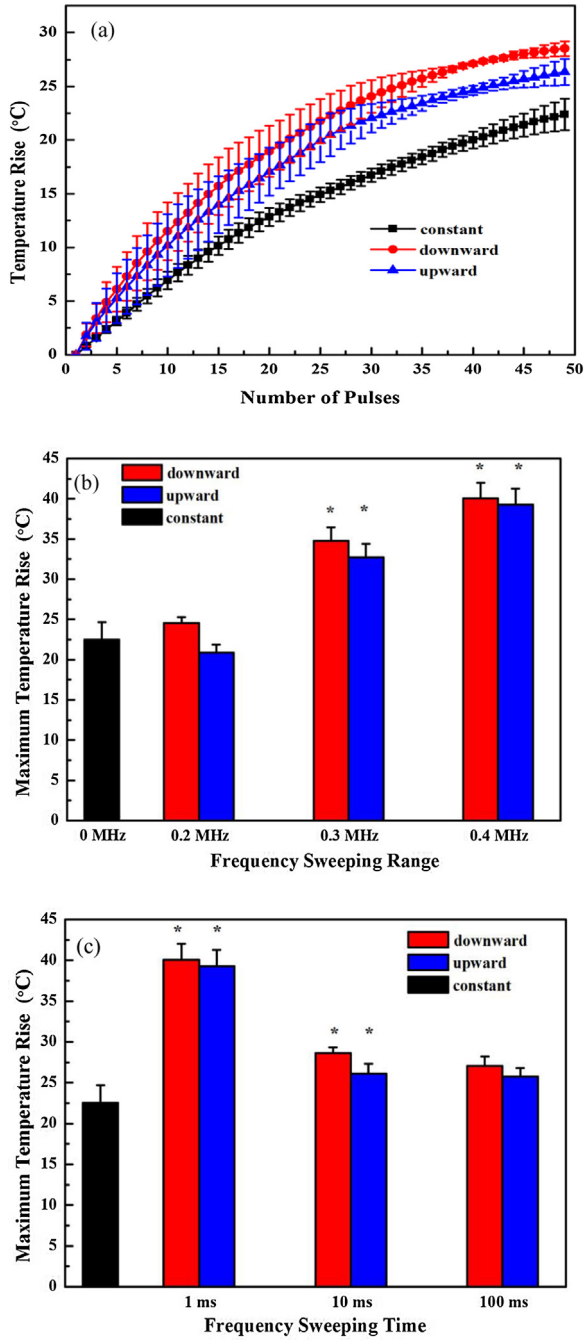


**Fig. 11.** (a) The temperature rise at the focus measured in the ex vivo porcine muscle with the different excitations (constant frequency, and downward and upward frequency chirps at the frequency sweeping frequency of 0.4 MHz in 1 ms), comparison of the maximum temperature rise using the varied (b) frequency sweeping ranges from 0.2 MHz to 0.4 MHz in 1 ms and (c) frequency sweeping times from 1 ms to 100 ms at the frequency sweeping range of 0.4 MHz at the end of 50 HIFU pulses (*: $p < 0.05$ in comparison to those lesion generation at the constant frequency).

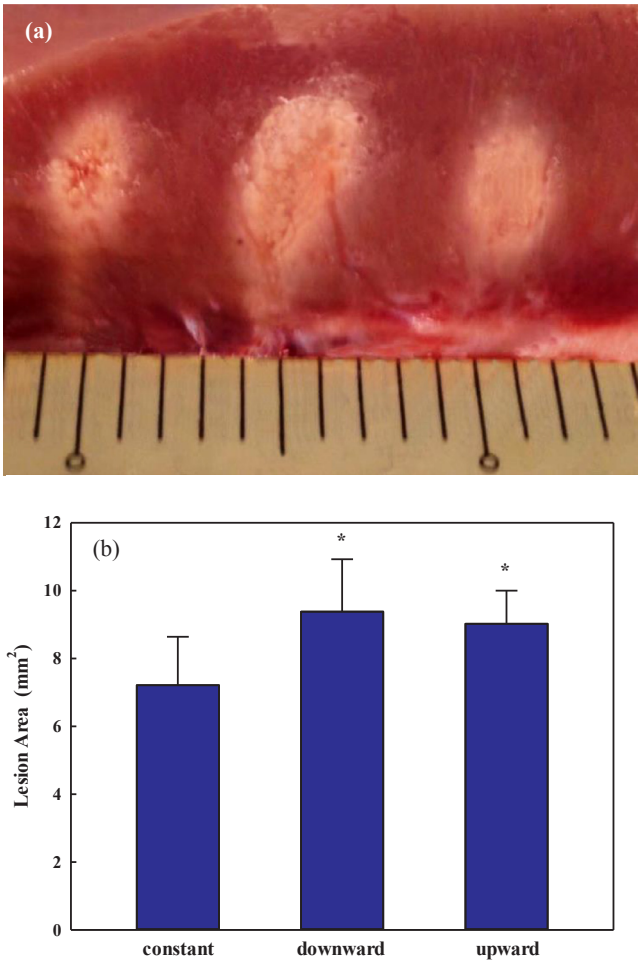


**Fig. 12.** (a) Representative photos of lesions in the porcine kidney samples using the constant frequency excitation, downward frequency chirp, and upward frequency chirp after 1 min-HIFU exposure (from left to right), and (b) comparison of the lesion areas. Frequency sweeping range and time are 0.4 MHz and 1 ms, respectively. *: statistical difference with the constant frequency excitation, $p < 0.05$.

filter was applied to the sub-harmonic and ultra-harmonics of measured PCD signals to quantify the scattering effect, and those broadband noises in the FFT spectra were for the IC level. In comparison to STFT methods, the derived IC levels are similar, but not the scattering effect, which is due to the larger width of the bandpass filter than the spread of harmonics of frequency chirps (see Fig. 8). However, PCD signals do not show a reliable correlation with the variation of lesion size and cannot provide the spatial information of cavitation. The current PCD setup only provides cavitation activities along the axial direction, but not in the other directions. To have a full view of the bubble cavitation, other monitoring methods, such as 2D arrays detectors [43] and the Doppler bubble images [44], are required.

Lesion enhancement depends on not only the sweeping time but also the frequency range employed which was limited by the bandwidth of the HIFU transducer. The current frequency range was only 0.4 MHz (12% of the central frequency and the variation of electrical-to-acoustic energy conversion efficiency of only 1 dB. It is expected that transducer with large fractional bandwidth will further enhance the lesion enhancement. Recent advances in the piezo-composite transducer technology could achieve 30–70% bandwidth with the maximum acoustic intensity of 30 W/cm$^2$ at the surface [45]. Faster sweeping is preferred in the lesion enhancement, which may be due to more number of abrupt transitions in the pressure amplitude and driving frequency at the same duration of HIFU exposure. However, the frequency sweeping direction seems to have little influence although downward sweeping is slightly better but without statistical difference.

There are several limitations of this study. Firstly, the KZK equation is only applicable to *F*-number larger than 1.3 at the constant frequency. The Westervelt equation in the time domain will be applied to simulate the acoustic field more accurately. Secondly, the presence of elasticity in the tissue may constrain the bubble expansion and increase

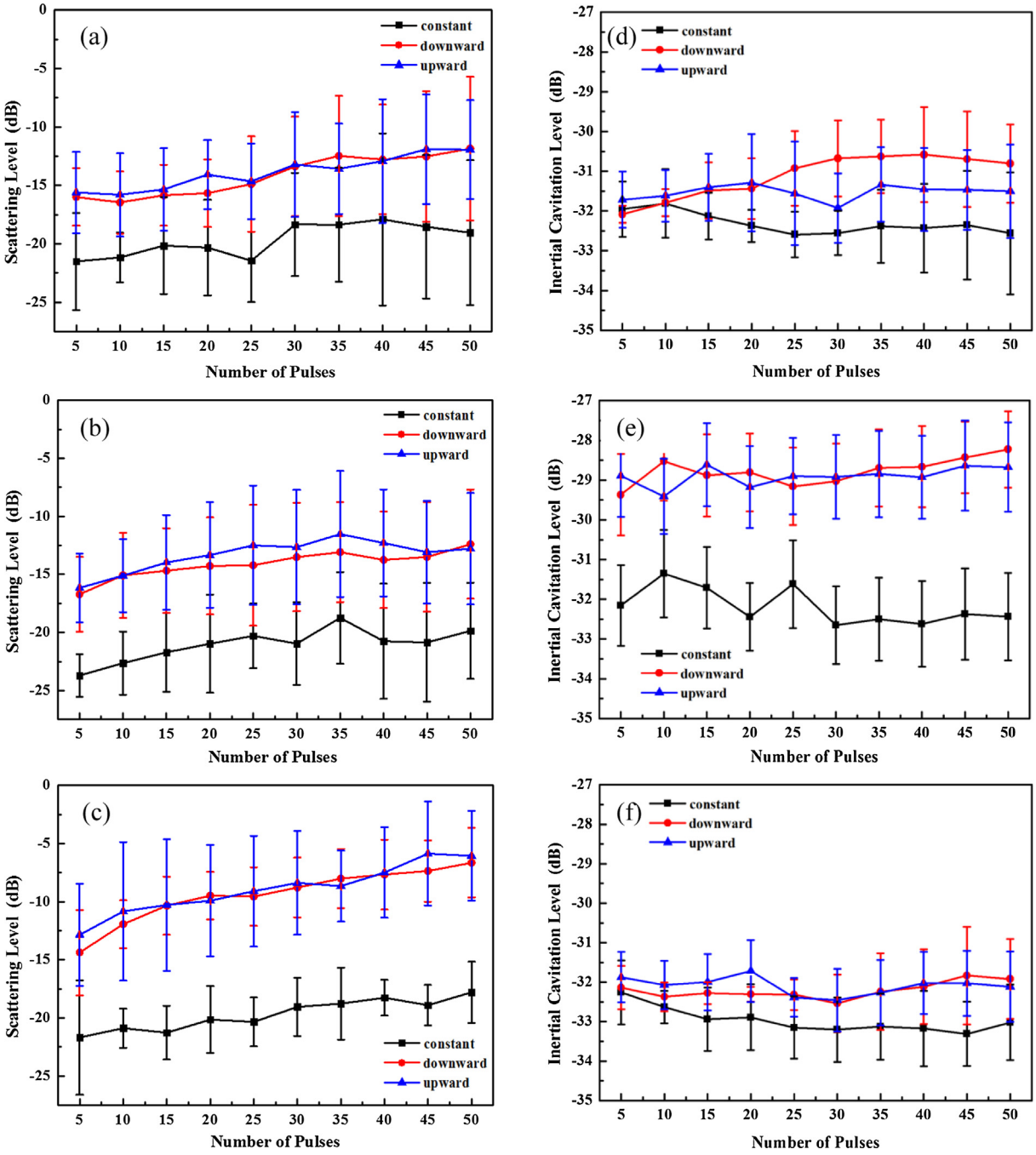


**Fig. 13.** The scattering level with the progress of HIFU exposure in the *ex vivo* porcine muscle with the frequency sweeping range of (a) 0.2 MHz, (b) 0.3 MHz, (c) 0.4 MHz in 1 ms, and the corresponding inertial cavitation levels from (d) to (f).

the threshold pressure for a bubble to oscillate inertially. The Keller-Miksis equation can be combined with the Voigt viscoelastic model to account for the strain-stress relation, and only the viscous damping term needs to be modified [46]. Thirdly, due to the heavy computation burden, the HIFU duration was limited to only 100 μs with a small range of parameters (e.g., delivered acoustic power, frequency sweeping range and time, and initial and uniform bubble size). More parametric exploration, including spatial distribution of bubble size in the focal region, will be carried out to optimize the operation. Fourthly, the high-speed imaging could provide direct evidence of the mechanism of frequency chirp excitations and the differences between their induced cavitation. Finally, the peak pressure of HIFU bursts at the focus is dependent on the driving frequency so that their envelope using frequency chirp excitation is not flat. By adjusting the driving amplitude at different frequencies it is possible to generate flat HIFU envelope and then evaluate the effect of frequency change on the bubble dynamics, cavitation-enhanced heating, and lesion production.

## 5. Conclusion

The numerical simulation shows that the frequency chirps can produce similar acoustic field as that using the constant frequency, but higher temperature elevations due to cavitation-enhanced heating. The temperature rises measured by the thermocouple and the produced

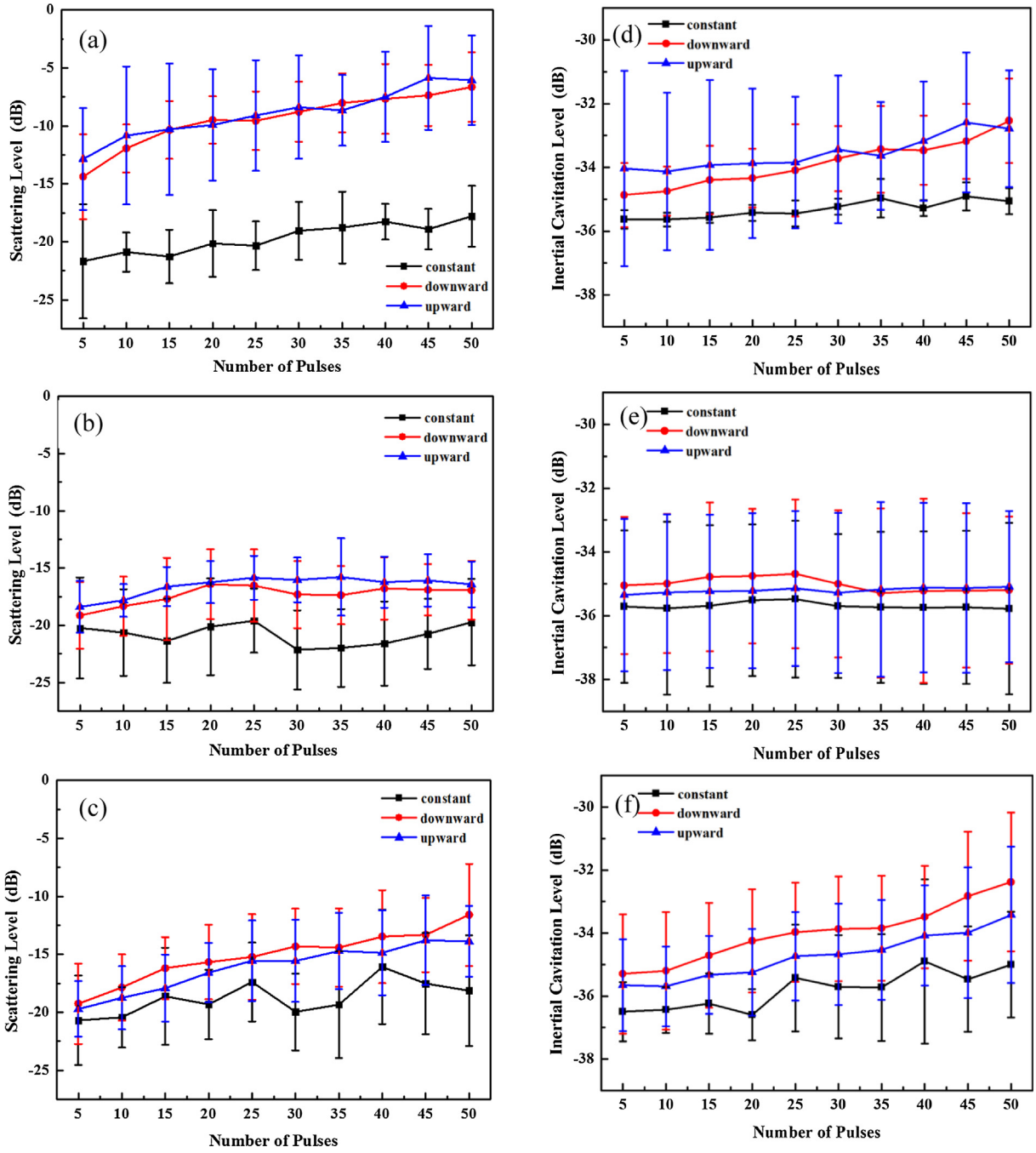


**Fig. 14.** The scattering level with the progress of HIFU exposure in the *ex vivo* porcine muscle with the frequency sweeping time of (a) 1 ms, (b) 10 ms, (c) 100 ms at the frequency sweeping range of 0.4 MHz, and the corresponding inertial cavitation levels from (d) to (f).

lesion in the gel phantom and *ex vivo* tissue samples were found to be improved using the frequency chirps. With a proper selection of the frequency sweeping range and time, a 50% enlargement of lesion size could be achieved. The mechanism of temperature and lesion enhancement is assumed to associate with the bubble cavitation in the focal region, which is confirmed by both scattering and inertial cavitation levels from the PCD signals measured during HIFU exposure. The frequency sweeping time plays a more critical role in the gel phantom while the frequency sweeping range more important in the tissue. However, frequency sweeping direction does not make a significant difference. In summary, short sweeping time and large frequency sweeping range are preferable for the enhancement of bubble cavitation and lesion production in HIFU ablation.

## References

[1] Y.-F. Zhou, High intensity focused ultrasound in clinical tumor ablation, World J. Clin. Oncol. 2 (2011) 8–27.
[2] T.J. Dubinsky, C. Cuevas, M.K. Dighe, O. Kolokythas, J.H. Hwang, High-intensity focused ultrasound: current potential and oncologic applications, Am. J. Roentgenol. 190 (2008) 191–199.
[3] R. Illing, J. Kennedy, F. Wu, G. Ter Haar, A. Protheroe, P. Friend, F. Gleeson, D. Cranston, R. Phillips, M. Middleton, The safety and feasibility of extracorporeal high-intensity focused ultrasound (HIFU) for the treatment of liver and kidney tumours in a Western population, Br. J. Cancer 93 (2005) 890–895.
[4] C.J. Diederich, K. Hynynen, Ultrasound technology for hyperthermia, Ultrasound Med. Biol. 25 (1999) 871–887.
[5] G. ter Haar, I. Rivens, L. Chen, S. Riddler, High intensity focused ultrasound for the treatment of rat tumours, Phys. Med. Biol. 36 (1991) 1495.
[6] G. ter Haar, D. Robertson, Tissue destruction with focused ultrasound in vivo, Eur.

Urol. 23 (1992) 8–11.
[7] C.C. Coussios, C.H. Farny, G. Ter Haar, R.A. Roy, Role of acoustic cavitation in the delivery and monitoring of cancer treatment by high-intensity focused ultrasound (HIFU), Int. J. Hyperth. 23 (2009) 105–120.
[8] S. Sokka, R. King, K. Hynynen, MRI-guided gas bubble enhanced ultrasound heating in in vivo rabbit thigh, Phys. Med. Biol. 48 (2003) 223.
[9] R.G. Holt, R.A. Roy, Measurements of bubble-enhanced heating from focused, MHz-frequency ultrasound in a tissue-mimicking material, Ultrasound Med. Biol. 27 (2001) 1399–1412.
[10] C. Coussios, C. Farny, G. ter Haar, R. Roy, Role of acoustic cavitation in the delivery and monitoring of cancer treatment by high-intensity focused ultrasound (HIFU), Int. J. Hyperth. 23 (2007) 105–120.
[11] Y.-S. Tung, H.-L. Liu, C.-C. Wu, K.-C. Ju, W.-S. Chen, W.-L. Lin, Contrast-agent-enhanced ultrasound thermal ablation, Ultrasound Med. Biol. 32 (2006) 1103–1110.
[12] S.-G. Zheng, H.-X. Xu, H.-R. Chen, Nano/microparticles and ultrasound contrast agents, World J. Radiol. 5 (2013) 468.
[13] J. Kwan, S. Graham, R. Myers, R. Carlisle, E. Stride, C. Coussios, Ultrasound-induced inertial cavitation from gas-stabilizing nanoparticles, Phys. Rev. E 92 (2015) 023019.
[14] P.S. Sheeran, S.H. Luois, L.B. Mullin, T.O. Matsunaga, P.A. Dayton, Design of ultrasonically-activatable nanoparticles using low boiling point perfluorocarbons, Biomaterials 33 (2012) 3262–3269.
[15] Q. Jin, S.-T. Kang, Y.-C. Chang, H. Zheng, C.-K. Yeh, Inertial cavitation initiated by polytetrafluoroethylene nanoparticles under pulsed ultrasound stimulation, Ultrason. Sonochem. 32 (2016) 1–7.
[16] R. Takagi, S. Yoshizawa, S.-I. Umemura, Enhancement of localized heating by ultrasonically induced cavitation in high intensity focused ultrasound treatment, Jpn. J. Appl. Phys. 49 (2010) 07HF21.
[17] X. Yang, J. Jo, Enhanced cavitation by using two consecutive ultrasound waves at different frequencies, Appl. Phys. Lett. 105 (2014) 193701.
[18] A. Brotchie, R. Mettin, F. Grieser, M. Ashokkumar, Cavitation activation by dual-frequency ultrasound and shock waves, PCCP 11 (2009) 10029–10034.
[19] L. Hallez, J. Lee, F. Touyeras, A. Nevers, M. Ashokkumar, J.-Y. Hihn, Enhancement and quenching of high-intensity focused ultrasound cavitation activity via short frequency sweep gaps, Ultrason. Sonochem. 29 (2016) 194–197.
[20] H. Kamimura, S. Wang, S. Wu, M. Karakatsani, C. Acosta, A. Carneiro, E. Konofagou, Chirp-and random-based coded ultrasonic excitation for localized blood-brain barrier opening, Phys. Med. Biol. 60 (2015) 7695.
[21] M. Wang, Y. Zhou, High-intensity focused ultrasound (HIFU) ablation by the frequency chirp excitation: reduction of the grating lobe in axial focus shifting, J. Phys. D Appl. Phys. 51 (2018) 285402.
[22] J.E. Soneson, A user-friendly software package for HIFU simulation, in: 8th International Symposium on Therapeutic Ultrasound, AIP Publishing, 2009, pp. 165–169.
[23] F.R. Gilmore, The growth or collapse of a spherical bubble in a viscous compressible liquid, Report No. 26-4 California Institute of Technology, Pasadena, CA, 1952, pp. 1–40.
[24] A. Eller, H. Flynn, Rectified diffusion during nonlinear pulsations of cavitation bubbles, J. Acoustical Soc. Am. 37 (1965) 493–503.
[25] H.H. Pennes, Analysis of tissue and arterial blood temperatures in the resting human foreman, J. Appl. Physiol. 1 (1948) 93–122.
[26] Y. Kaneko, J.S. Allen, S. Yoshizawa, Y. Matsumoto, Heating mechanism of microbubbles and bubble properties, in: Ultrasonics Symposium, 2004 IEEE, IEEE, 2004, pp. 882–885.
[27] S. Zhu, P. Zhong, Shock wave–inertial microbubble interaction: A theoretical study based on the Gilmore formulation for bubble dynamics, J. Acoust. Soc. Am. 106 (1999) 3024–3033.
[28] C. Lafon, V. Zderic, M.L. Noble, J.C. Yuen, P.J. Kaczkowski, O.A. Sapozhnikov, F. Chavrier, L.A. Crum, S. Vaezy, Gel phantom for use in high-intensity focused ultrasound dosimetry, Ultrasound Med. Biol. 31 (2005) 1383–1389.
[29] Y. Zhou, L. Zhai, R. Simmons, P. Zhong, Measurement of high intensity focused ultrasound fields by a fiber optic probe hydrophone, J. Acoust. Soc. Am. 120 (2006) 676.
[30] Y. Zhou, X.W. Gao, Variations of bubble cavitation and temperature elevation during lesion formation by high-intensity focused ultrasound, J. Acoust. Soc. Am. 134 (2013) 1683–1694.
[31] T. Li, H. Chen, T. Khokhlova, Y.N. Wang, W. Kreider, X. He, J.H. Hwang, Passive cavitation detection during pulsed HIFU exposures of ex vivo tissues and in vivo mouse pancreatic tumors, Ultrasound Med. Biol. 40 (2014) 1523–1534.
[32] C.D. Arvanitis, M. Bazan-Peregrino, B. Rifai, L.W. Seymour, C.C. Coussios, Cavitation-enhanced extravasation for drug delivery, Ultrasound Med. Biol. 37 (2011) 1838–1852.
[33] Y. Zhou, X. Wilson Gao, Variations of bubble cavitation and temperature elevation during lesion formation by high-intensity focused ultrasound, J. Acoust. Soc. Am. 134 (2013) 1683–1694.
[34] K.B. Bader, C.K. Holland, Gauging the likelihood of stable cavitation from ultrasound contrast agents, Phys. Med. Biol. 58 (2013) 127–144.
[35] J.M. Borsboom, C.T. Chin, A. Bouakaz, M. Versluis, N. de Jong, Harmonic chirp imaging method for ultrasound contrast agent, IEEE Trans. Ultrason. Ferroelectr. Freq. Control 52 (2005) 241–249.
[36] J. Chapelon, F. Dupenloup, H. Cohen, P. Lenz, Reduction of cavitation using pseudorandom signals IEEE transactions on ultrasonics, ferroelectrics, and frequency control, 43 (1996) 623–625.
[37] M. Bailey, V. Khokhlova, O. Sapozhnikov, S. Kargl, L. Crum, Physical mechanisms of the therapeutic effect of ultrasound (a review), Acoust. Phys. 49 (2003) 369–388.
[38] Y.-N. Wang, T. Khokhlova, M. Bailey, J.H. Hwang, V. Khokhlova, Histological and biochemical analysis of mechanical and thermal bioeffects in boiling histotripsy lesions induced by high intensity focused ultrasound, Ultrasound Med. Biol. 39 (2013) 424–438.
[39] A. Brotchie, F. Grieser, M. Ashokkumar, Effect of power and frequency on bubble-size distributions in acoustic cavitation, Phys. Rev. Lett. 102 (2009) 084302.
[40] C.C. Coussios, R.A. Roy, Applications of acoustics and cavitation to noninvasive therapy and drug delivery, Annu. Rev. Fluid Mech. 40 (2008) 395–420.
[41] M.S. Canney, V.A. Khokhlova, O.V. Bessonova, M.R. Bailey, L.A. Crum, Shock-induced heating and millisecond boiling in gels and tissue due to high intensity focused ultrasound, Ultrasound Med. Biol. 36 (2010) 250–267.
[42] C.H. Farny, R.G. Holt, R.A. Roy, The correlation between bubble-enhanced HIFU heating and cavitation power, IEEE Trans. Biomed. Eng. 57 (2010) 175–184.
[43] V.A. Salgaonkar, S. Datta, C.K. Holland, T.D. Mast, Passive cavitation imaging with ultrasound arrays, J. Acoust. Soc. Am. 126 (2009) 3071–3083.
[44] T. Li, T.D. Khokhlova, O.A. Sapozhnikov, M. O'Donnell, J.H. Hwang, A new active cavitation mapping technique for pulsed HIFU applications-bubble doppler, IEEE Trans. Ultrason. Ferroelectr. Freq. Control 61 (2014) 1698–1708.
[45] G. Fleury, D.M. de Lima, K. Hynynen, R. Berriet, O. Le Baron, B. Huguenin, New piezocomposite transducers for therapeutic ultrasound, in: Biomedical Optics 2003, International Society for Optics and Photonics, 2003, pp. 227–236.
[46] X. Yang, C.C. Church, A model for the dynamics of gas bubbles in soft tissue, J. Acoust. Soc. Am. 118 (2005) 3595–3606.